Calculated quasiparticle and optical properties of orthorhombic and cubic Ca_2Si

S. Lebègue,[1] B. Arnaud,[2] and M. Alouani[3]
[1]*Department of Physics, Uppsala University, SE-75121 Uppsala, Sweden*
[2]*Groupe Matière condensée et Matériaux (GMCM), Campus de Beaulieu-Bat 11A 35042 Rennes cedex, France*
[3]*Institut de Physique et de Chimie des Matériaux de Strasbourg (IPCMS), UMR 7504 CNRS-ULP, 23 rue du Loess, 67034 Strasbourg, France*

(Received 8 March 2005; published 1 August 2005)

The quasiparticle properties of a technologically important material Ca_2Si is studied by means of the all electron GW approximation based on the projector-augmented-wave method (PAW). Both the orthorhombic and the cubic phases are explored, and the resulting band structures are compared with those obtained in the framework of the local-density approximation (LDA) of the density functional theory. An improved energy band gap for both phases of this material is compared to experiment. The dielectric function is also computed for both phases, and its shown that the quasiparticle self-energy correction and the local-field effects strongly affect the optical spectra and the static dielectric function. The analysis of the locations of the Brillouin zone **k** points and the interband transitions responsible of the main peak is conducted for both phases.

DOI: 10.1103/PhysRevB.72.085103 PACS number(s): 71.15.Mb, 71.20.Nr

I. INTRODUCTION

Metal silicides have recently the subject of extensive studies to improve the understanding of their structural, electronic, and optical properties due to their possible technological applications. Among this wide family of compounds, the so-called "Kankyo semiconductors"[1] play an increasing role in a device's fabrication because they are composed of naturally abundant and less toxic elements. In particular, Ca_2Si is considered to be a promising candidate for applications, and hence many experimental studies, like photoemission[2] and inverse photoemission[3] experiments as well as resistivity[4] measurements have been performed on this material. Recently, the growth of microstructures of semiconducting silicide layers made of Ca_2Si was reported,[5,6] and their excellent compatibility with existent silicon based technology was pointed out.[6]

Many theoretical studies were conducted to understand the various experimental data. However, the results were rather contradictory since, for example, Bisi and co-workers[2] have shown that Ca_2Si is a semimetal, whereas a semiconducting behavior was found by Imai *et al.*[7] In order to clarify the situation, Migas and co-workers[8] performed a study of the structural, electronic, and optical properties of Ca_2X ($X=Si,Ge,Sn,Pb$) compounds in the framework of the density functional theory (DFT) in the local-density approximation (LDA).[9,10] In particular, they identified the stable crystalline structure of Ca_2Si to be of the simple orthorhombic type in agreement with x-ray diffraction experiments. However, their results concerning the electronic and optical properties are subject to caution due to the well-known problem of the DFT to deal with excited states. Their results must be viewed only as a preliminary step towards the understanding of the electronic structure of these interesting materials.

Regarding the potential applications related to Ca_2Si, a clear answer must, therefore, be provided concerning the calculated quasiparticle band structure, and should be compared to available photoemission and inverse photoemission experiments. The knowledge of the band gap of this material, i.e., its value and its nature (direct versus indirect) as well as its optical properties are of extreme importance for optoelectronic applications.

The GW approximation (GWA) of Hedin,[11,12] where the quasiparticle self-energy is approximated as the product of the LDA Green's function G and the screened Coulomb interaction W, is becoming the tool of choice for computing the excited states of materials. The purpose of this study is, therefore, to present our results concerning the quasiparticle and optical properties of Ca_2Si within this framework.

Our paper is organized as follows: In the second section we investigate the structural properties of Ca_2Si in the cubic and orthorhombic structures by means of the all-electron projector-augmented-wave method (PAW).[13] Then, we present our quasiparticle band structures obtained within the GWA and finally in the third section we study the dielectric function for both phases of Ca_2Si. In particular, we discuss the importance of the self-energy correction and local-field (LF) effects on the computed optical spectra and analyze the main peaks in calculated optical spectra.

II. ELECTRONIC PROPERTIES

A. Structural properties

The ground state electronic structure properties of Ca_2Si are calculated within the DFT.[9,10] The exchange-correlation potential has been determined within the generalized gradient approximation (GGA),[14] and the Kohn-Sham equations are solved using the PAW method. This method combines an all-electron description of the wave functions within a molecular dynamic formalism.[13] All internal coordinates have been relaxed and a Parrinello-Rahman simulation has been used to optimize the unit cell. The orthorhombic unit cell contains 12 atoms and is depicted in Fig. 1.

To insure convergence of the total energy, a mesh of $6\times8\times4$ **k** points in the full Brillouin zone (BZ) and an energy cutoff of 25 Ryd for the plane-wave basis set have been

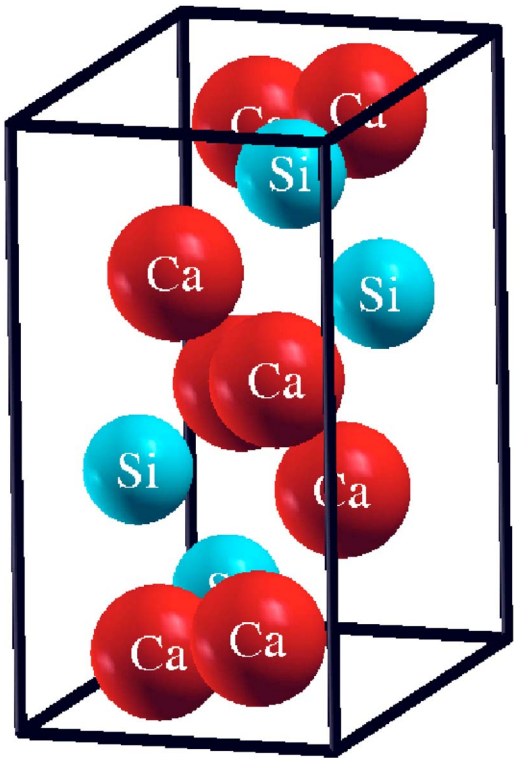

FIG. 1. (Color online) Unit cell of the orthorhombic phase of Ca_2Si. It contains 12 atoms per cell and the calcium are distributed on two inequivalent sites.

used in our calculations for the orthorhombic phase. A mesh of $11\times11\times11$ **k** points and an energy cutoff of 20 Ryd was used for the cubic phase. This phase crystallizes in the well-known antifluorite structure (not shown here), where the silicon is placed at the origin whereas the two equivalent calcium atoms are at $(1/4,1/4,1/4)$ and $(-1/4,-1/4,-1/4)$. Although the cubic phase is not the most stable one, it is also important to investigate its properties since it can probably be easily grown under hydrostatic pressure.[8]

The resulting lattice parameters are presented in Table I and compared to other available results. Our values are in good agreement with available results, showing the ability of the PAW method to compete with other *ab initio* schemes. The structural properties of this system have been extensively studied in Ref. 8, so we will not add any further comments and prefer to focus on the excited properties which are treated in the next subsection.

TABLE I. Calculated lattice parameters (in Angstroms) of the orthorhombic and cubic phases of Ca_2Si compared with other theoretical (Ref. 8) using the ultrasoft pseudopotential approximation (USPP) and experimental results (Refs. 15 and 16).

	a	*b*	*c*
Orthorhombic phase (this work)	7.664	4.799	9.002
Orthorhombic phase[a]	7.618	4.793	9.001
Orthorhombic phase[b]	7.667	4.799	9.002
Orthorhombic phase[c]	7.691	4.816	9.035
Cubic phase (this work)	7.149		
Cubic phase[a]	7.148		

[a]USPP results of Ref. 8.
[b]Experimental results Ref. 15.
[c]Experimental results of Ref. 16.

B. Quasiparticle properties

As presented in the introduction, we use the GWA to the self-energy[11,12] to overcome the difficulty of the DFT in dealing with excited state properties. This method has been used successfully in the past for a wide range of materials.[17–19] Within this method, quasiparticle (QP) equations replace the usual Kohn-Sham ones, and the QP energies $E_n(\mathbf{k})$ and QP wave functions $\psi_{\mathbf{k}n}(\mathbf{r})$ are obtained by solving the QP equations

$$(T+V_{ext}+V_h)\psi_{\mathbf{k}n}(\mathbf{r})+\int d^3r'\Sigma(\mathbf{r},\mathbf{r}',E_n(\mathbf{k}))\psi_{\mathbf{k}n}(\mathbf{r}')$$
$$=E_n(\mathbf{k})\psi_{\mathbf{k}n}(\mathbf{r}), \quad (1)$$

where T, V_{ext}, V_h, and Σ are, respectively, the kinetic energy operator, the external potential due to the ion cores, the average electrostatic (Hartree) potential, and the electron self-energy operator. In the case of the GWA, the self-energy is simply the product of the one-electron Green's function G and the screened Coulomb interaction W:[11,12]

$$\Sigma(\mathbf{r},\mathbf{r}',\omega)=\frac{i}{2\pi}\int d\omega' G(\mathbf{r},\mathbf{r}',\omega+\omega')e^{i\delta\omega'}W(\mathbf{r},\mathbf{r}',\omega'), \quad (2)$$

where δ is a positive infinitesimal. In order to get a practical scheme, the quasiparticle energies $E_n(\mathbf{k})$ are obtained by a first-order expansion of the self-energy:

$$\mathrm{Re}\,E_n(\mathbf{k})=\epsilon_n(\mathbf{k})+Z_{n\mathbf{k}}\times[\langle\Psi_{\mathbf{k}n}|\mathrm{Re}\,\Sigma(\mathbf{r},\mathbf{r}',\epsilon_n(\mathbf{k}))|\Psi_{\mathbf{k}n}\rangle$$
$$-\langle\Psi_{\mathbf{k}n}|V_{xc}^{\mathrm{LDA}}(r)|\Psi_{\mathbf{k}n}\rangle]. \quad (3)$$

The renormalization factor $Z_{n\mathbf{k}}$ is defined by

$$Z_{n\mathbf{k}}=\left[1-\langle\Psi_{\mathbf{k}n}|\frac{\partial}{\partial\omega}\mathrm{Re}\,\Sigma(\mathbf{r},\mathbf{r}',\omega=\epsilon_n(\mathbf{k}))|\Psi_{\mathbf{k}n}\rangle\right]^{-1}. \quad (4)$$

The screened Coulomb interaction W is calculated in two ways: For the cubic phase (3 atoms per unit cell) the random-phase approximation (RPA) is used as described in Ref. 20, but for the orthorhombic phase one needs to compute the quasiparticle energies for a system of 12 atoms per unit cell, and this approximation becomes computationally expensive. We have, therefore, resorted to the plasmon-pole (PlP) model which avoid the calculation of the full dielectric function (see Ref. 21 for a complete description). Apart from the fact that the imaginary part of the self-energy is not accessible with the PlP, this approximation produces quasiparticle energies in good agreement with the full GW-RPA for "*sp*" materials. A slight overestimation of the interband transitions could occur in some materials, see Ref. 20.

In Fig. 2 we present the QP band structure for the orthorhombic phase along some high-symmetry directions. To en-

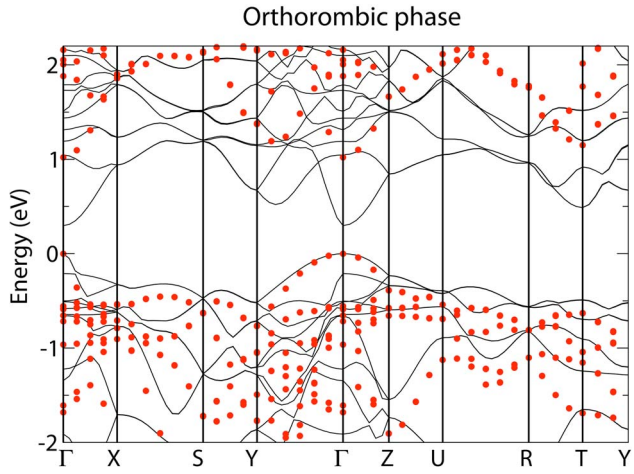

FIG. 2. (Color online) DFT band structure (full lines) and quasiparticle corrections (red dots) for the orthorhombic phase of Ca_2Si. The DFT top of valence state is at the zero of the energy scale.

sure well-converged quantities, we have used 24 **k**-points in the full BZ as well as 300 bands, and a dielectric matrix of size 561×561. A detailed overview of the DFT and QP energies is given in Table II. From the data presented in this table, we can notice that the difference of energies between the conduction and valence states are substantially increased by the use of the GWA as compared to the DFT results. In particular, the minimum band gap (corresponding to interband transitions at the Γ point) is 1.02 eV within the GWA, whereas its only 0.30 eV within the DFT, i.e., its is more than three times larger. This DFT value is in good agreement with the value of 0.35 eV reported by Migas *et al.*[8] Our agreement with the results of Migas and co-workers rules out the possibility of a semimetallic behavior as proposed earlier.[2] On the other hand, our value of 1.02 eV is much smaller than the estimated value of 1.90 eV from resistivity measurements.[4] Although the GWA leads sometimes to a slightly underestimated interband transitions for semiconductors,[20] the overall agreement between calculated and experimental results is, in general, rather quite satisfactory and a large difference of 0.9 eV is clearly unexpected and might be related to possible problems with the samples used in Ref. 4. At this point, additional information is required to resolve this discrepancy. We provide, therefore, in Table II the relevant information for future detailed analysis.

We have also carried out GWA calculations of the cubic phase of Ca_2Si. We used 64 **k** points in the full BZ and 200 bands. For the computation of the screened Coulomb interaction we used a dielectric matrix of size 331×331 for each **k** point. The value of the minimum band gap obtained within the DFT is 0.50 eV and is in good agreement with the value of 0.56 eV reported in Ref. 8. The GWA provided a value of 1.16 eV (see Table III for all the values of the calculated interband transitions). It is interesting to notice that the last valence band at the high-symmetry point X is almost equal to the K point value within the DFT, whereas the X, L, and some points along the $K \rightarrow \Gamma$ are all equal within the GWA, making the exact nature of the band gap hard to determine, as pictured in Fig. 3. However, this particular feature could be used to make this material switchtable between direct and indirect band gap upon applying pressure or growth on a suitable substrate. In addition, it is also interesting to notice that the GWA correction depends strongly on the character of the bands. For example, at the Γ point, the difference of the first and the second doubly degenerate conduction bands is

TABLE II. Quasiparticle interband transitions at some high symmetry points, Γ, S, Y, Z, U, R, and T of the BZ of the Ca_2Si in its orthorhombic phase. The values corresponding to the minimum band gap are underlined.

	Orthorhombic phase	
	DFT	GWA
$\mathbf{\Gamma}_v \rightarrow \mathbf{\Gamma}_{1c}$	<u>0.30</u>	<u>1.02</u>
$\mathbf{\Gamma}_v \rightarrow \mathbf{\Gamma}_{2c}$	1.05	1.88
$\mathbf{X}_v \rightarrow \mathbf{X}_{1c}$	1.26	2.45
$\mathbf{X}_v \rightarrow \mathbf{X}_{2c}$	1.56	2.41
$\mathbf{S}_v \rightarrow \mathbf{S}_{1c}$	1.67	2.78
$\mathbf{S}_v \rightarrow \mathbf{S}_{2c}$	1.98	3.45
$\mathbf{Y}_{8v} \rightarrow \mathbf{Y}_{1c}$	1.20	2.15
$\mathbf{Y}_{8v} \rightarrow \mathbf{Y}_{2c}$	1.67	2.93
$\mathbf{Z}_{8v} \rightarrow \mathbf{Z}_{1c}$	1.08	2.05
$\mathbf{Z}_{8v} \rightarrow \mathbf{Z}_{2c}$	1.74	3.18
$\mathbf{U}_{8v} \rightarrow \mathbf{U}_{1c}$	1.44	2.55
$\mathbf{U}_{8v} \rightarrow \mathbf{U}_{2c}$	1.61	2.65
$\mathbf{R}_{8v} \rightarrow \mathbf{R}_{1c}$	1.53	2.58
$\mathbf{R}_{8v} \rightarrow \mathbf{R}_{2c}$	1.81	3.08
$\mathbf{T}_{8v} \rightarrow \mathbf{T}_{1c}$	0.98	1.78
$\mathbf{T}_{8v} \rightarrow \mathbf{T}_{2c}$	1.41	2.40

TABLE III. Quasiparticle interband transitions at the high symmetry points L, Γ, X, W, and K for the cubic phase of Ca_2Si. The values corresponding to the minimum band gap are underlined.

	Cubic phase	
	DFT	GWA
$\mathbf{L}_v \rightarrow \mathbf{L}_{1c}$	2.42	3.37
$\mathbf{L}_v \rightarrow \mathbf{L}_{2c}$	2.64	3.25
$\mathbf{\Gamma}_v \rightarrow \mathbf{\Gamma}_{1c}$	2.10	2.31
$\mathbf{\Gamma}_v \rightarrow \mathbf{\Gamma}_{2c}$	2.16	3.27
$\mathbf{X}_v \rightarrow \mathbf{X}_{1c}$	<u>0.50</u>	<u>1.16</u>
$\mathbf{X}_v \rightarrow \mathbf{X}_{2c}$	1.55	2.63
$\mathbf{W}_v \rightarrow \mathbf{W}_{1c}$	1.37	2.27
$\mathbf{W}_v \rightarrow \mathbf{W}_{2c}$	2.78	3.99
$\mathbf{K}_v \rightarrow \mathbf{K}_{1c}$	0.93	1.69
$\mathbf{K}_v \rightarrow \mathbf{K}_{2c}$	2.25	3.40

about 0.06 eV within the DFT, this difference becomes 0.96 eV within the GWA. This can be explained by the fact that the first band is of pure *sp* character at the Γ point, whereas the second one is of pure *d* character. The effect of the correction is therefore to push the *d* band towards higher energies. This effect is also reproduced when using the PlP approximation for the cubic phase (results not presented here). The dependence of the correction upon band character has been already observed before for LiBC and related materials[22] and is related to the degree of localization of the orbitals to be corrected by the self-energy. This points out once again the importance of using a GWA scheme rather than the more traditional LDA or GGA approximation to compute the excited state properties of materials.

III. OPTICAL PROPERTIES

A. Method of calculation

Optical spectroscopy is becoming a widely used tool to probe the electronic properties of materials. To compare the calculated optical spectra with experiments, the computation should include quasiparticle corrections, as obtained in the previous section, and the local-field effects. None of these effects were included in previous work.[8] In this study it will be shown that some of these effects are of particular importance and can drastically change the optical spectra. The formalism used in this work is shortly reviewed.

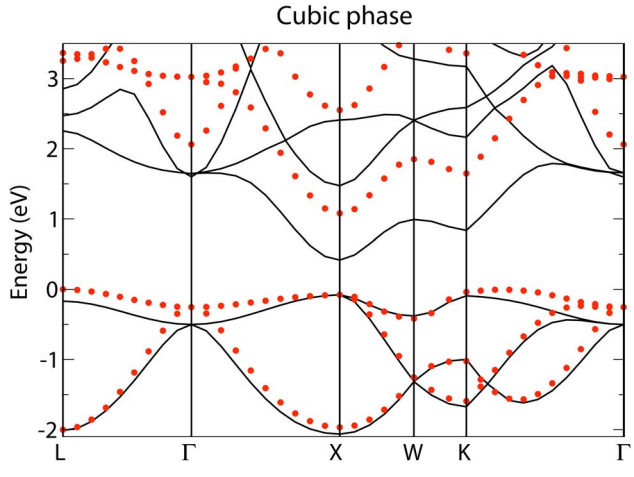

FIG. 3. (Color online) DFT band structure (full lines) and GWA quasiparticle corrections (red dots) for the cubic phase of Ca_2Si. The DFT top of the valence state is located at the zero of the energy scale.

The macroscopic dielectric function is defined as

$$\epsilon(\omega) = \lim_{\mathbf{q}\to 0} \frac{1}{[\epsilon^{-1}_{\mathbf{G},\mathbf{G}'}(\mathbf{q},\omega)]_{\mathbf{0},\mathbf{0}}} \tag{5}$$

which can be rewritten as:

$$\epsilon(\omega) = \lim_{\mathbf{q}\to 0} \epsilon_{0,0}(\mathbf{q},\omega) - \lim_{\mathbf{q}\to 0} \sum_{\mathbf{G},\mathbf{G}'\neq 0} \epsilon_{\mathbf{0},\mathbf{G}}(\mathbf{q},\omega)\epsilon^{-1}_{\mathbf{G},\mathbf{G}'}(\mathbf{q},\omega)\epsilon_{\mathbf{G}',0}(\mathbf{q},\omega) \tag{6}$$

The first term of Eq. (6) is the interband contribution without LF effects, whereas the second one represents the LF field contribution. The LF represent the explicit dependence of the dielectric function $\epsilon(\mathbf{r},\mathbf{r}',\omega)$ on $\mathbf{r}$ and $\mathbf{r}'$ and not only on $|\mathbf{r}-\mathbf{r}'|$.[23,24] Therefore, the local fields cannot be neglected in systems with strong inhomogeneities of the charge density. In our case the random phase approximation (RPA) to the

TABLE IV. Effects of the local fields and the quasiparticle shift on the macroscopic static dielectric constant for both the orthorhombic and cubic phases. Here *xx*, *yy*, and *zz* denote the three independent components of the dielectric function of the orthorhombic phase, and *av* represents the averaged value of the static dielectric function for a useful comparison with the value for the cubic phase presented in the last line.

	DFT	DFT+LF	QP shift	QP shift+LF
ϵ_∞^{xx} orthorhombic	18.4	15.2	13.8	11.7
ϵ_∞^{yy} orthorhombic	18.1	14.3	13.2	10.8
ϵ_∞^{zz} orthorhombic	17.7	13.5	13.5	10.8
ϵ_∞^{av} orthorhombic	18.1	14.3	13.4	11.1
ϵ_∞ cubic	14.7	11.5	11.1	9.0

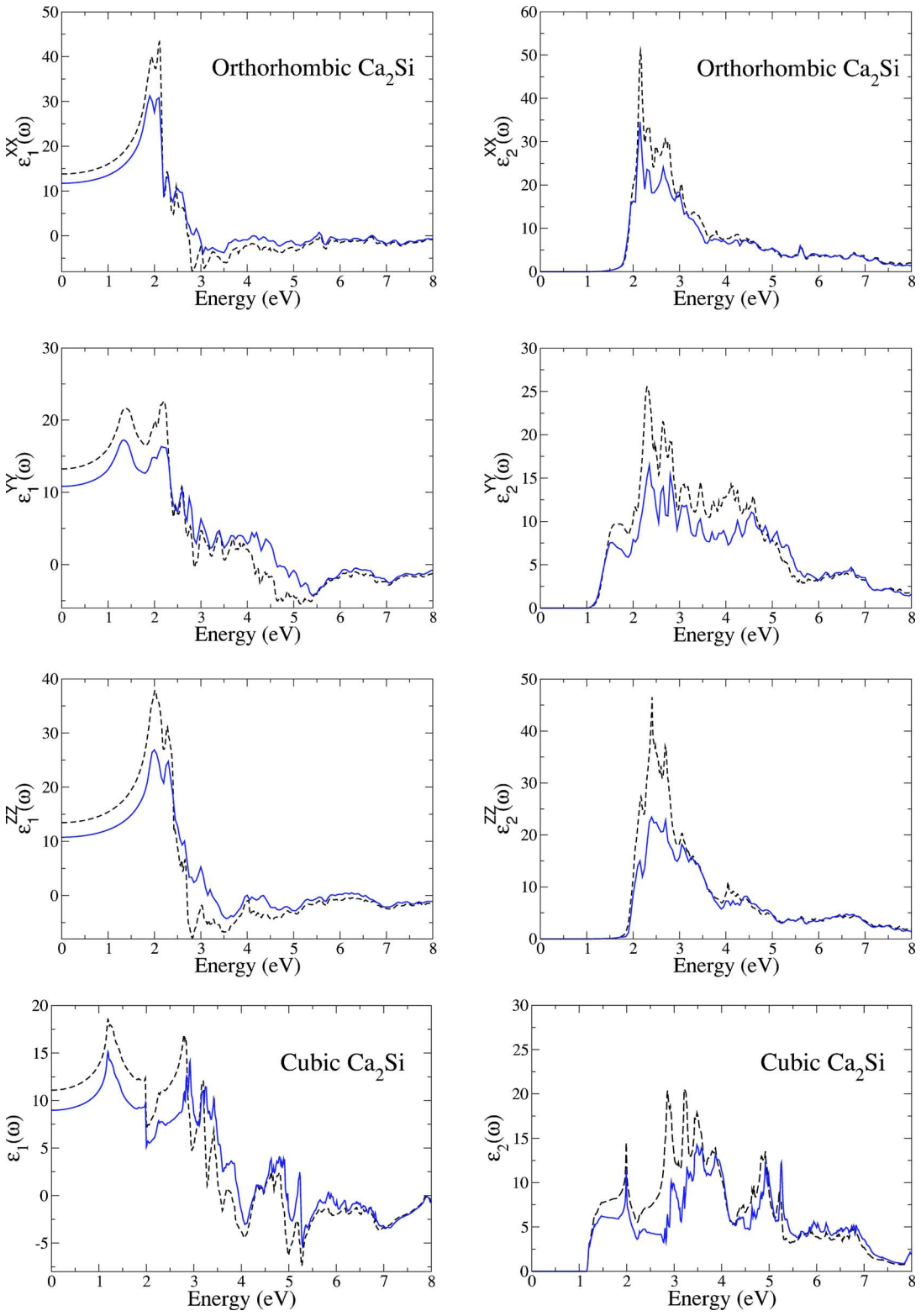

FIG. 4. (Color online) Real (upper row) and imaginary (lower row) parts of the dielectric function for both the orthorhombic and cubic phases of Ca_2Si. In the case of the orthorhombic phase, the spectra for the three polarizations of light (along the x, y, and z directions) are given. The plots with full lines (in blue) include the local-field effects and those with dashed lines do not. In all calculations, the effect of the self-energy correction has been accounted for by shifting the conduction states so that the GWA minimum band gap is reproduced.

dielectric function is used, and according to Adler and Wiser[25–27] the dielectric function $\epsilon_{\mathbf{G},\mathbf{G}'}(\mathbf{q},\omega)$ can be given by

$$\epsilon_{\mathbf{G},\mathbf{G}'}(\mathbf{q},\omega) = \delta_{\mathbf{G},\mathbf{G}'} - \frac{8\pi}{\Omega|\mathbf{q}+\mathbf{G}||\mathbf{q}+\mathbf{G}'|} \times \sum_{l,m,\mathbf{k}} \frac{[n_{l\mathbf{k}-\mathbf{q}} - n_{m\mathbf{k}}] M_{\mathbf{G}}^{lm}(\mathbf{k},\mathbf{q})[M_{\mathbf{G}'}^{lm}(\mathbf{k},\mathbf{q})]^*}{\epsilon_{l\mathbf{k}-\mathbf{q}}^{qp} - \epsilon_{m\mathbf{k}}^{qp}, + \omega + i\delta} \tag{7}$$

where $n_{m\mathbf{k}}$ and $\epsilon_{m\mathbf{k}}^{qp}$ are, respectively, the occupation number and the one-particle energy for a given state specified by the band index m and the wave vector $\mathbf{k}$. Also, δ is a positive infinitesimal, and the matrix elements $M_{\mathbf{G}}^{lm}(\mathbf{k},\mathbf{q})$ are given by

$$M_{\mathbf{G}}^{lm}(\mathbf{k},\mathbf{q}) = \langle \Psi_{\mathbf{k}-\mathbf{q}l} | e^{-i(\mathbf{q}+\mathbf{G})\mathbf{r}} | \Psi_{\mathbf{k}m} \rangle \tag{8}$$

In our case, the imaginary part of the dielectric function (ϵ_2) is calculated first by using tetrahedron method[28,29] to integrate over the Brillouin zone. Then the real part of $\epsilon(\omega)$ is obtained using a Kramers-Kronig transformation. More details about the implementation can be found elsewhere.[30]

B. Results and discussions

Concerning the quasiparticle correction, since a calculation of the self-energy for all the **k** points and all the bands involved in Eq. (7) is computationally overwhelming, we have chosen to apply a constant shift to the unoccupied DFT bands in order to produce an average GWA correction to the band structure. This shift is chosen as the correction done by the GWA to the minimum DFT band gap: 0.72 eV for the orthorhombic phase and 0.66 eV for the cubic phase (see Tables II and III). This correction is crucial to insure that our results can be compared with future experimental data. One should stress out that this energy shift of the DFT eigenvalues will not fully reproduce the quasiparticle energies of the conduction states because as it was pointed before the GWA correction depends on whether the band is localized or delocalized. Nonetheless, we expect that the use of the correct quasiparticle energies instead of the DFT shifted energies will bring only minor corrections to the dielectric function that can hardly be noticed in the calculated optical spectra.

The calculated static dielectric constants in various approximations (with or without GWA correction to the one-particle energies and with or without LF effects) are presented in Table IV. In both phases, Ca_2Si is characterized by a large value of the static dielectric function. In particular, the orthorhombic phase is found to be more polarizable than the cubic phase, regardless the approximation used to perform the calculation. This is easily understood by noticing that the DFT band gap of the orthorhombic phase is smaller than the one of the cubic phase, leading to a value of the dielectric constant of 18.1 (averaged value over the three directions) compared to a value of 14.7 for the cubic phase. This trend is also confirmed when using QP energies instead of the DFT one to compute the dielectric constant. However, the difference between the two values is reduced compared to the previous DFT ones. This reduction originates from the fact that the average GWA correction is more important for orthorhombic phase than for cubic phase, bringing both phases to almost the same value of the minimum band gap.

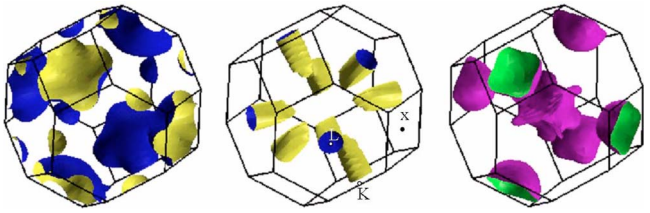

FIG. 5. (Color online) Representation of the **k** point locations of the interband transitions responsible of the main peaks in the imaginary part of the dielectric function (ϵ_2) of the cubic phase. Left: Those for the last occupied band to the first conduction band at the energy of the first peak of ϵ_2. Middle: Those for the last occupied band to the first conduction band at the energy of the second peak of ϵ_2. Right: Those for the last occupied band to the second conduction band at the energy of the second peak of ϵ_2.

The static dielectric function is a ground state property and, therefore, one expects that the calculation using the DFT one particle energies and including the LF effects will be much closer to experiment. The dielectric constant including QP correction are only relevant if they are also corrected for excitonic effects. This is because the excitonic effects shift back the oscillator strength towards lower photon energies, canceling partially or totally the QP correction to the static dielectric function. Unfortunately, the effects of the electron-hole interaction on the static dielectric constant cannot be obtained accurately at the present moment because of computational difficulties in the convergence process of the of the optical spectra within this approach (see Ref. 30 for further details).

In Fig. 4, the frequency dependent dielectric function of the two phases are represented. All the spectra shown here include the QP corrections[31] with (full line) or without (dashed line) LF effects. The size of the dielectric matrix [see Eq. (7)] is a crucial parameter for a converged calculation of the LF effects. In our case, we found that a dielectric function matrix of 69×69 is sufficient to ensure convergence. For the orthorhombic phase, we have used a grid of $6\times8\times4$ **k** points for the head element and a grid of $4\times6\times2$ k points for the wings and the body elements, whereas for the cubic phase of Ca_2Si grids of, respectively, $20\times20\times20$ **k** points and $10\times10\times10$ **k** points were sufficient. As for the static dielectric function case, the frequency dependent computed dielectric function for the orthorhombic phase shows a sizable anisotropy for the three independent polarizations of light. In particular, the spectrum for $E\|a$ and $E\|c$ are quite similar whereas the spectrum for $E\|b$ looks similar to the one of the cubic phase. As noticed in Ref. 8 for their LDA calculations, this originates from the different projections of the crystalline structure with respect to a given direction. Here we show that this analysis still holds when including LF and QP correction in the calculation of the spectra, which is far from obvious since LF account for the nonhomogeneity of the charge density. For all spectra, the LF effects reduce the intensity of the peaks, but do not change significantly their positions.

In order to improve our understanding of the optical spectra, it is useful to determine the **k** point locations of the

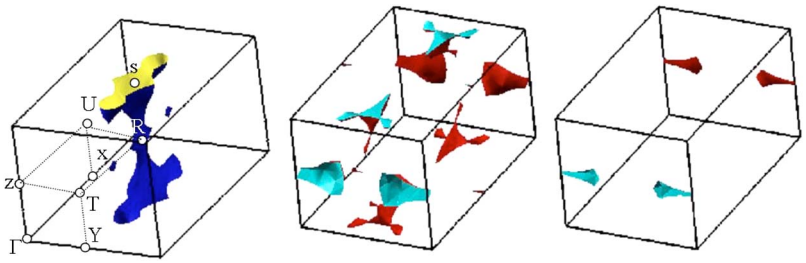

FIG. 6. (Color online) Representation of the **k** point locations for the interband transitions responsible for the first peaks of ϵ_2 of the orthorhombic phase ϵ_2. Left: Those for the last occupied band and the first conduction band at the energy of the main peak of ϵ_2 for $E\|a$ (2.16 eV). Middle: Those for the last occupied band to the third conduction band at the energy of the main peak of ϵ_2 for $E\|b$ (2.37 eV). Right: Those for the last occupied band to the third conduction band at the energy of the main peak of ϵ_2 for $E\|c$ (2.42 eV). The Γ high-symmetry point is located at every corner.

interband transitions responsible of the main peaks in the imaginary part of the dielectric function. The prime effect of the momentum matrix elements is to allow or forbid some interband transitions according to dipolar selection rules. In the case of Ca_2Si, the last valence bands are mainly of "*p*" character (from the silicon atomic species) whereas the first conduction bands have mainly "*d*" character (from the calcium atomic species); the effects of the momentum matrix elements consist mainly in modulating the oscillator strength of each transition.

To obtain both band to band transitions and a **k**-point analysis of the structures in the optical spectra, we reported the values of interband transitions for the whole BZ and selected different energies corresponding to the main peaks in ϵ_2. Strictly speaking this analysis provides only the **k** point locations and interband transitions responsible of the structures in the joint density of states (JDOS), however, since we know the selection rules and the character of the occupied and empty bands, this analysis remains valid for the optical spectra. Our analysis is presented in Fig. 5 in the case of the cubic phase. On the left plot, the **k** point locations of the interband transitions between the last occupied band and the first empty conduction band responsible of the first peak (1.96 eV) of ϵ_2 are represented. Clearly, this peak originates from interband transitions in the vicinity of the *X* and *K* high-symmetry points of the BZ. This is also understood by looking at the band structure of the cubic phase (see Fig. 3): The minimum of transitions is located at the high symmetry *X* point with a second minimum at the *K* point. In the middle and right part of Fig. 5, we present **k**-point locations for the interband transitions responsible of the second peak (2.85 eV) of the dielectric function, respectively, from the last valence band to the first and second conduction bands. Both interband transitions along a direction parallel to *L*-Γ (middle plot) and interband transitions around *X* and Γ points (right plot) contribute to this peak. Other interband transitions do not contribute to this structure.

For the orthorhombic phase, the interband transitions and **k** point locations of the peaks in ϵ_2 are by far more complicated than for the cubic phase due to the large number of sub-bands involved in the analysis. We choose, therefore, to analyze only the lowest interband transitions responsible of the main peak in ϵ_2 for the three components, corresponding to light polarization along the *x*, *y*, or *z* directions. Concerning the $E\|a$ case, the **k** point locations for the interband transitions between the last valence band and the first conduction band responsible for the peak at 2.16 eV are represented by the left plot of Fig. 6. The major contribution comes from the interband transitions along the high-symmetry direction *S*-*R* together with some along the *S*-*Y* line. On the other hand, the locations of the **k** points for the interband transitions responsible for the main peak at 2.37 eV in $\epsilon_2^{yy}(\omega)$ are represented by the second picture of Fig. 6 and are shown to be issued by excitations around the *Z*-*T* and *S*-*Y* high symmetry directions. In this case, transitions from the last valence band to the two first conduction bands do not contribute to this peak because it is lying at much higher energies, so we have represented transitions to the third unoccupied state. This is also the case when $E\|c$, for which the main peak is located at 2.42 eV. From the right plot of Fig. 6, we conclude that transitions around the *Z*-*T* lines are important. Of course there is a lot of other relevant transitions to be analyzed in order to have a complete understanding of the whole structure in the optical spectra. But a full analysis of the structures in calculated spectra is without much value in the absence of experimental data. However, we believe that our work will be helpful for the interpretation of future optical experiments. Here we just want to show that the information provided by a plot of the location of the **k** points of the interband transitions responsible of the structures in the optical spectra, as seen in Fig. 6 is much nicer to understand than directly analyzing the complicated orthorhombic band structure plot by inspection to extract the relevant information.

IV. CONCLUSION

In summary, we have presented results concerning *ab initio* quasiparticle properties and optical spectra for a technological important material Ca_2Si in both its orthorhombic and cubic phases. We have given precise values of electronic interband transitions within the GWA and calculated the optical spectra including both LF effects and quasiparticle shifts. The results using the GWA are shown to differ markedly from the DFT results and might be in better agreement with future experimental data. The main structures in the optical spectra are analyzed and the locations of the **k** points of the interband transitions responsible of these

peaks are obtained. The path is now open for new experimental work to compare with our results.

It is also of interest to compute the excited states properties for some related materials like Ca_2Ge, Ca_2Sn, Ca_2Pb. Their properties have been studied in Ref. 8 within the LDA but to our knowledge no GW calculations are published in the literature. Another point of particular importance is the study of excitonic effects on the optical spectra. They can affect the overall shape of the spectra in a quite significant way. At the present time the excitonic effects are computationally time consuming and, therefore, the calculations are prohibitive for materials with many atoms per unit cell.

ACKNOWLEDGMENT

Supercomputer time was provided by CINES (project gem1100) on the IBM SP4.

[1] *Symposium on Silicide Kankyo Semiconductors-Ecologically Friendly Semiconductors-Opto-electronic and Energy Research for Next Generation Thin Solid Films, Special Issues, Volume 381, Issue 2* (2001).
[2] O. Bisi, L. Braicovich, C. Carbone, I. Lindau, A. Iandelli, G. L. Olcese, and A. Palenzona, Phys. Rev. B **40**, 10194 (1989).
[3] C. Chemelli, M. Sancrotti, L. Braicovich, F. Ciccacci, O. Bisi, A. Iandelli, G. L. Olcese, and A. Palenzona, Phys. Rev. B **40**, 10210 (1989).
[4] G. Busch, P. Junod, U. Katz, and U. Winkler, Helv. Phys. Acta **27**, 193 (1954).
[5] H. Tatsuoka, N. Takagi, S. Okaya, Y. Sato, T. Inaba, T. Ohishi, A. Yamamoto, T. Matsuyama, and H. Kuwabara, Thin Solid Films **461**, 57 (2004).
[6] L. I. Ivanenko, V. L. Shaposhnikov, A. B. Filonov, A. V. Krivosheeva, V. E. Borisenko, D. B. Migas, L. Miglio, G. Behr, and J. Schumann, Thin Solid Films **461**, 141 (2004).
[7] Y. Imai and A. Watanabe, Intermetallics **10**, 333 (2002).
[8] D. B. Migas, L. Miglio, V. L. Shaposhnikov, and V. E. Borisenko, Phys. Rev. B **67**, 205203 (2003).
[9] P. Hohenberg and W. Kohn, Phys. Rev. **136**, B864 (1964).
[10] W. Kohn and L. Sham, Phys. Rev. **140**, A1133 (1965).
[11] L. Hedin, Phys. Rev. **139**, A796 (1965).
[12] L. Hedin, and S. Lundquist, in *Solid State Physics*, edited by H. Ehrenreich, F. Seitz, and D. Turnbull (Academic, New York, 1969), Vol. 23, p. 1.
[13] P. E. Blöchl, Phys. Rev. B **50**, 17953 (1994).
[14] J. P. Perdew, K. Burke, and M. Ernzerhof, Phys. Rev. Lett. **77**, 3865 (1996).
[15] P. Eckerlin and E. Wlfel, Z. Anorg. Chem. **280**, 321 (1955).
[16] P. Manfrinetti, M. Fornasini, and A. Palenzona, Intermetallics **8**, 223 (2000).
[17] F. Aryasetiawan and O. Gunnarsson, Rep. Prog. Phys. **61**, 237 (1998).
[18] W. G. Aulbur, L. Jönsson, and J. W. Wilkins, Solid State Phys. **54**, 1 (1999).
[19] G. Onida, L. Reining, and A. Rubio, Rev. Mod. Phys. **74**, 601 (2002).
[20] S. Lebègue, B. Arnaud, M. Alouani, and P. E. Bloechl, Phys. Rev. B **67**, 155208 (2003).
[21] B. Arnaud and M. Alouani, Phys. Rev. B **62**, 4464 (2000).
[22] S. Lebègue, B. Arnaud, P. Rabiller, M. Alouani, and W. E. Pickett, Europhys. Lett. **68**, 846 (2004).
[23] M. S. Hybertsen and S. G. Louie, Phys. Rev. B **35**, 5585 (1987).
[24] M. S. Hybertsen and S. G. Louie, Phys. Rev. B **35**, 5602 (1987).
[25] S. D. Adler, Phys. Rev. **126**, 413 (1962).
[26] N. Wiser, Phys. Rev. **129**, 62 (1963).
[27] D. L. Johnson, Phys. Rev. B **9**, 4475 (1974).
[28] O. Jepsen and O. K. Andersen, Solid State Commun. **9**, 1763 (1971).
[29] G. Lehmann and M. Taut, Phys. Status Solidi B **54**, 469 (1972).
[30] B. Arnaud and M. Alouani, Phys. Rev. B **63**, 085208 (2001).
[31] In the framework of the DFT, our spectra are the same as the ones presented by Migas and co-workers, therefore, we have not included them for comparison.